

Efficient hierarchical clustering for continuous data

Ricardo Henao and Joseph E. Lucas

November 13, 2021

Abstract

We present a new sequential Monte Carlo sampler for coalescent based Bayesian hierarchical clustering. Our model is appropriate for modeling non-i.i.d. data and offers a substantial reduction of computational cost when compared to the original sampler without resorting to approximations. We also propose a quadratic complexity approximation that in practice shows almost no loss in performance compared to its counterpart. We show that as a byproduct of our formulation, we obtain a greedy algorithm that exhibits performance improvement over other greedy algorithms, particularly in small data sets. In order to exploit the correlation structure of the data, we describe how to incorporate Gaussian process priors in the model as a flexible way to model non-i.i.d. data. Results on artificial and real data show significant improvements over closely related approaches.

Keywords: coalescent, gaussian process, sequential Monte Carlo, greedy algorithm.

1 Introduction

Learning hierarchical structures from observed data is a common practice in many knowledge domains. Examples include phylogenies and signaling pathways in biology, language models in linguistics, etc. Agglomerative clustering is still the most popular approach to hierarchical clustering due to its efficiency, ease of implementation and a wide range of possible distance metrics. However, because it is algorithmic in nature, there is no principled way to that agglomerative clustering can be used as a building block in more complex models. Bayesian priors for structure learning on the other hand, are perfectly suited to be employed in larger models. As an example, several authors have proposed using hierarchical structure priors to model correlation in factor models (Rai and Daume III, 2009; Henao et al., 2012; Zhang et al., 2011).

Ricardo Henao is Postdoctoral Associate and Joseph E. Lucas is Assistant Research Professor at the Institute for Genome Sciences and Policy (IGSP), Duke University, Durham, NC 27710. E-mail: r.henao@duke.edu and joe@stat.duke.edu. This work was supported by funding from the Defense Advanced Research Projects Agency (DARPA), number IN66001-07-C-0092 (G.S.G.)

There are many approaches to hierarchical structure learning already proposed in the literature, see for instance Neal (2003a); Heller and Ghahramani (2005); Teh et al. (2008); Adams et al. (2010). Since we are particularly interested in continuous non i.i.d. data and model based hierarchical clustering we will focus our work on the Bayesian agglomerative clustering model proposed by Teh et al. (2008). Although the authors introduce priors both for continuous and discrete data, no attention is paid to the non i.i.d. case, mainly because their work is focused in proposing different inference alternatives.

The approach proposed by Teh et al. (2008) is a Bayesian hierarchical clustering model with coalescent priors. Kingman’s coalescent is a standard model from population genetics perfectly suited for hierarchical clustering since it defines a prior over binary trees (Kingman, 1982a,b). This work advances Bayesian hierarchical clustering in two ways: (i) we extend the original model to handle non i.i.d. data and (ii) we propose an efficient sequential Monte Carlo inference procedure for the model which scales quadratically rather than cubically as in the original sampler by Teh et al. (2008). As a byproduct of our approach we propose as well a small correction to the greedy algorithm of Teh et al. (2008) that shows gains particularly in small data sets.

There is a separate approach by Görür and Teh (2009) that also improves the cubic computational cost of Bayesian hierarchical clustering. They introduce an efficient sampler with quadratic cost that although proposed for discrete data can be easily extended to continuous data, however as we will show, our approach is still substantially faster.

The remainder of the manuscript is organized as follows, the data model and the use of coalescents as priors for hierarchical clustering are reviewed in Section 2. Our approach to inference and relationships to previous approaches are described in Section 3. Section 4 contains numerical results on both artificial and real data. Section 5 concludes with a discussion and perspectives for future research.

2 Coalescents for hierarchical clustering

A model for hierarchical clustering consists of learning about a nested set of partitions of n observations in d dimensions, \mathbf{X} . Assuming that each partition differs only by two elements, the set of partitions defines a binary tree with n leaves and $n - 1$ branching points. Defining $\mathbf{t} = [t_1 \dots t_{n-1}]$ and $\boldsymbol{\pi} = \{\pi_1, \dots, \pi_{n-1}\}$ as the vector of branching times and the set of partitions, respectively, we can write a Bayesian model for hierarchical clustering as

$$\begin{aligned} \mathbf{x}_i | \mathbf{t}, \boldsymbol{\pi} &\sim p(\mathbf{x}_i | \mathbf{t}, \boldsymbol{\pi}), \\ \mathbf{t}, \boldsymbol{\pi} &\sim \text{Coalescent}(n), \end{aligned} \tag{1}$$

where \mathbf{x}_i is the i -th row of \mathbf{X} , $p(\mathbf{x}_i | \mathbf{t}, \boldsymbol{\pi})$ is its likelihood and the pair $\{\mathbf{t}, \boldsymbol{\pi}\}$ is provided with a prior distribution over binary tree structures known as the coalescent.

2.1 Kingman's coalescent

The n -coalescent is a continuous-time Markov chain originally introduced to describe the common genealogy of a sample of n individuals backwards in time (Kingman, 1982a,b). It defines a prior over binary trees with n leaves, one for each individual. The coalescent assumes a uniform prior over tree structures, $\boldsymbol{\pi}$, and exponential priors on the set of $n - 1$ merging times, \mathbf{t} .

It can be thought of as a generative process on partitions of $\{1, \dots, n\}$ as follows

- Set $k = 1$, $t_0 = 0$, $\pi_0 = \{\{1\}, \dots, \{n\}\}$.
- While $k < n$
 - Draw $\Delta_k \sim \text{Exponential}((n - k + 1)(n - k)/2)$ (rate parameter).
 - Set $t_k = t_{k-1} + \Delta_k$.
 - Merge uniformly two sets of π_{k-1} into π_k .
 - Set $k = k + 1$.

Because there are $(n - k + 1)(n - k)/2$ possible merges at stage K , any particular pair in π_i merges with prior rate 1 for any i . We can compute the prior probability of a particular configuration of the pair $\{\mathbf{t}, \boldsymbol{\pi}\}$ as

$$p(\mathbf{t}, \boldsymbol{\pi}) = \prod_{k=1}^{n-1} \exp\left(-\frac{(n-k+1)(n-k)}{2}\Delta_k\right), \quad (2)$$

this is, the product of merging and coalescing time probabilities. Some properties of the n -coalescent include: (i) the marginal distribution of $\boldsymbol{\pi}$ is uniform and independent of \mathbf{t} , (ii) it is exchangeable in the set of partitions π_i for every i and (iii) the expected value of t_{n-1} (last coalescing time) is $\mathbb{E}[t_{n-1}] = 2(1 - n^{-1})$.

2.1.1 Distribution of the latent nodes

Let $z_k^* \in \pi_i$ be a node in a binary tree with associated d -dimensional vector \mathbf{z}_k , and let $z_{c_1}^*$ and $z_{c_2}^*$ be its children. We designate the leaves of the tree with x_i^* . If we define $p(\mathbf{z}_k | \mathbf{z}_c, \mathbf{t}, \cdot)$ to be the transition density between a child node, \mathbf{z}_c , and its parent, \mathbf{z}_k , then we can recursively define $q(\mathbf{z}_k | \boldsymbol{\pi}, \mathbf{t}, \cdot)$ to be a (possibly unnormalized) distribution of \mathbf{z}_k as follows:

$$\begin{aligned} q(\mathbf{x}_i | \boldsymbol{\pi}, \mathbf{t}, \cdot) &= \delta_{\mathbf{x}_i}, \\ q(\mathbf{z}_k | \boldsymbol{\pi}, \mathbf{t}, \cdot) &= \prod_{c \in C} \int p(\mathbf{z}_k | \mathbf{z}_c, \mathbf{t}, \cdot) q(\mathbf{z}_c | \boldsymbol{\pi}, \mathbf{t}, \cdot) d\mathbf{z}_c, \\ &= Z_k(\mathbf{X}, \boldsymbol{\pi}, \mathbf{t}, \cdot) q'(\mathbf{z}_k | \boldsymbol{\pi}, \mathbf{t}, \cdot), \end{aligned}$$

where $C = \{c_1, c_2\}$ contains the two sets in π_{k-1} that merge in π_k and $q'(\mathbf{z}_k | \boldsymbol{\pi}, \mathbf{t}, \cdot)$ is a density (integrating to 1) and Z_k is the appropriate scaling factor.

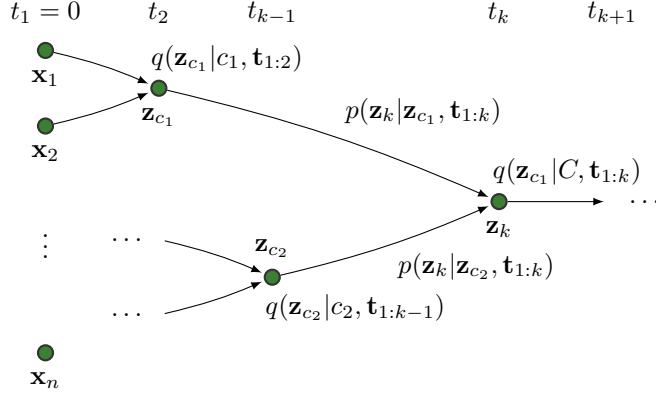


Figure 1: Binary tree structure. Latent variable \mathbf{t} and $\boldsymbol{\pi}$ define merging points and merging sets, respectively.

Recently, Teh et al. (2008) showed that by using an agglomerative approach for constructing $\{\mathbf{t}, \boldsymbol{\pi}\}$, the likelihood for the model in equation (1) can be recursively written as

$$p(\mathbf{X}|\mathbf{t}, \boldsymbol{\pi}, \cdot) = \prod_{k=1}^{n-1} Z_k(\mathbf{X}|\boldsymbol{\pi}, \mathbf{t}, \cdot). \quad (3)$$

We note that, because of the tree structure, \mathbf{z}_k is independent of \mathbf{X} conditional on the distributions of its two child nodes. This implies that $Z_k(\mathbf{X}|\boldsymbol{\pi}, \mathbf{t}, \cdot) = Z_k(\mathbf{X}|\pi_k, \mathbf{t}_{1:k}, \cdot)$. Our formulation is equivalent to using *message passing* to marginalize recursively from the leaves to the root of the tree (Pearl, 1988). The message is $q(\mathbf{z}_k|\cdot)$ for node \mathbf{z}_k and it summarizes the entire subtree below node \mathbf{z}_k .

Figure 1 illustrate the process for a segment of a tree. The size of partitions π_k shrink as k increases, so from the illustration $\pi_1 = \{\{1\}, \{2\}, \dots, \{n\}\}$, $\pi_2 = \{\{1, 2\}, \dots, \{n\}\}$, $\pi_{k-1} = \{c_1, c_2, \dots\}$, $\pi_k = \{\{c_1, c_2\}, \dots\}$, $\pi_n = \{\{1, 2, \dots, n\}\}$.

The joint distribution needed to perform inference can be obtained by combining likelihood and prior in equations (3) and (2) as

$$p(\mathbf{X}, \mathbf{t}, \boldsymbol{\pi}, \cdot) = \prod_{k=1}^{n-1} \exp\left(-\frac{(n-k+1)(n-k)}{2}\Delta_k\right) Z_k(\mathbf{X}|\pi_k, \mathbf{t}_{1:k}, \cdot). \quad (4)$$

2.2 Gaussian transition distributions

We are interested in correlated continuous data, thus we assume a multivariate Gaussian distribution for the transition probability,

$$p(\mathbf{z}_k|\mathbf{z}_c, \mathbf{t}_{1:k}, \boldsymbol{\Phi}) = \mathcal{N}(\mathbf{z}_k|\mathbf{z}_c, \Delta_c \boldsymbol{\Phi}),$$

where $\boldsymbol{\Phi}$ is a covariance matrix encoding the correlation structure in \mathbf{z}_k and Δ_c is the time elapsed between t_k and t_c , not necessarily $t_{k-1} - t_k$ as can be seen in Figure 1. We

denote the time at which the set c was created as t_c . Individual terms of the likelihood in equation (3) can be computed using

$$\begin{aligned} q(\mathbf{z}_k | \pi_k, \mathbf{t}_{1:k}, \cdot) &= \mathcal{N}(\mathbf{z}_k | \mathbf{m}_{c_1}, \tilde{s}_{c_1} \Phi) \mathcal{N}(\mathbf{z}_k | \mathbf{m}_{c_2}, \tilde{s}_{c_2} \Phi), \\ &= Z_k(\mathbf{X} | \pi_k, \mathbf{t}_{1:k}, \cdot) \mathcal{N}(\mathbf{z}_k | s_k (\tilde{s}_{c_1}^{-1} \mathbf{m}_{c_1} + \tilde{s}_{c_2}^{-1} \mathbf{m}_{c_2}), s_k \Phi), \end{aligned}$$

where \mathbf{m}_{c_1} and s_{c_1} are mean and variance of $q(\mathbf{z}_k | \cdot)$, respectively, where $\tilde{s}_{c_1} = \Delta_{c_1} + s_{c_1}$, and where $\Delta_{c_1} = t_k - t_{c_1}$. This leads to $s_k = (\tilde{s}_{c_1}^{-1} + \tilde{s}_{c_2}^{-1})^{-1}$ and the normalization constant is

$$Z_k(\mathbf{X} | \pi_k, \mathbf{t}_{1:k}, \cdot) = (2\pi)^{-d/2} |v_k \Phi|^{-1/2} \exp\left(-\frac{1}{2}(\mathbf{m}_{c_1} - \mathbf{m}_{c_2}) v_k^{-1} \Phi^{-1} (\mathbf{m}_{c_1} - \mathbf{m}_{c_2})^\top\right),$$

where $v_k = \tilde{s}_{c_1} + \tilde{s}_{c_2} = 2\Delta_k + r_k$ and $r_k = 2t_{k-1} - t_{c_1} - t_{c_2} + s_{c_1} + s_{c_2}$. Note that $\Delta_{c_1} = \Delta_{c_2}$ only if c_1 and c_2 are singletons.

3 Inference

Inference is carried out using a sequential Monte Carlo (SMC) sampling based upon equation (4) (see Doucet et al., 2001). More precisely, for a set of M particles, we approximate the posterior of the pair $\{\mathbf{t}, \boldsymbol{\pi}\}$ using a weighted sum of point masses obtained iteratively by drawing coalescing times t_k and chain states π_k one at a time from their posterior as

$$p(\Delta_k, \pi_k | \mathbf{t}_{1:k}, \pi_{k-1}, \cdot) = Z_{k,C}^{-1} \exp\left(-\frac{(n-k+1)(n-k)}{2} \Delta_k\right) Z_k(\mathbf{X} | \pi_k, \mathbf{t}_{1:k}, \cdot), \quad (5)$$

where $Z_{k,C}^{-1}$ is the normalization constant and C is a pair of elements of π_{k-1} . In order to compute the weights required by SMC we need to compute $Z_{k,C}^{-1}$ for every pair in π_{k-1} .

Algorithms introduced by Teh et al. (2008) try to avoid the computational complexity of using equation (5) directly by simplifying it or by means of greedy alternatives. They propose for instance to draw Δ_k from the prior so computing $Z_{k,C}^{-1}$ is no longer necessary thus reducing the computational cost. From equation (5) we see that $Z_{k,C}^{-1}$ needs to be computed for every pair in π_{k-1} at every iteration of the sampler, simply because the rate of the exponential distribution is a function of k . We will show that by using some properties of the distributions involved in equation (5) we can effectively decrease the computational complexity of the SMC sampler with almost no performance penalty. In particular, we will show that the most expensive parts of $Z_{k,C}^{-1}$ need to be computed only once during inference.

We can expand the right hand side of equation (5) as

$$\begin{aligned} p(\Delta_k, \pi_k | \mathbf{t}_{1:k-1}, \pi_{k-1}, \cdot) & \propto Z_k(\mathbf{X} | \pi_k, \mathbf{t}_{1:k}, \cdot) \text{Exponential}(2\Delta_k + r_k | \lambda/2) \text{Exponential}(-r_k | \lambda/2), \\ & = Z_{k,C}^{-1} \text{GIG}(2\Delta_k + r_k | \tilde{\lambda}, \boldsymbol{\epsilon}_{k-1,C}, \lambda), \end{aligned} \quad (6)$$

where $\lambda = (n - k + 1)(n - k)/2$, $\tilde{\lambda} = 1 - d/2$, $\boldsymbol{\epsilon}_{k-1,C} = (\mathbf{m}_{c_1} - \mathbf{m}_{c_2})\boldsymbol{\Phi}^{-1}(\mathbf{m}_{c_1} - \mathbf{m}_{c_2})$, $C = \{c_1, c_2\} \in \pi_{k-1}$, $\text{GIG}(\lambda, \chi, \psi)$ is the generalized inverse Gaussian with parameters $\{\lambda, \chi, \psi\}$ (Jørgensen, 1982). This leads to

$$Z_{k,C} \propto \frac{K_{\tilde{\lambda}}(\sqrt{\lambda\boldsymbol{\epsilon}_{k-1,C}})}{(\lambda\boldsymbol{\epsilon}_{k-1,C}^{\tilde{\lambda}})^{\tilde{\lambda}/2}} \exp\left(\frac{\lambda}{2}r_k\right), \quad (7)$$

where $K_\nu(z)$ is the modified Bessel function of second kind (Abramowitz and Stegun, 1965). The details on how to obtain equations (6) and (7) can be found in Appendix A. From Equation (6) we have

$$\Delta_k | \pi_k, \mathbf{t}_{1:k-1}, \cdot \sim \text{GIG}(2\Delta_k + r_k | \tilde{\lambda}, \boldsymbol{\epsilon}_{k,C}, \lambda), \quad (8)$$

$$C^* | \pi_{k-1}, \mathbf{t}_{1:k-1}, \cdot \sim \text{Discrete}(C^* | \mathbf{w}_{k-1}), \quad (9)$$

where \mathbf{w}_{k-1} is the vector of normalized weights, ranging over all pairs, computed using equation (7) and C^* is the pair of π_{k-1} that gets merged in π_k . Sampling equations (7), (8) and (9) have useful properties, (i) the conditional posterior of π_k does not depend on Δ_k . (ii) Sampling from Δ_k amounts to draw from a truncated generalized inverse Gaussian distribution. (iii) We do not need to sample Δ_k for every pair in π_{k-1} , in fact we only need to do so for the merging pair C^* . (iv) Although λ in equation (7) changes with k , the most expensive computation, $\boldsymbol{\epsilon}_{k-1,C}$ needs to be computed only once. (v) The distribution in equation (7) has heavier tails than a Gaussian distribution and $Z_{k,C} \rightarrow \infty$ as $\boldsymbol{\epsilon}_{k-1,C} \rightarrow 0$ for $d > 1$. Furthermore, we can rewrite equation (7) as

$$Z_{k,C} \propto \frac{K_{d/2-1}(\sqrt{\lambda\boldsymbol{\epsilon}_{k-1,C}})}{(\lambda^{-1}\boldsymbol{\epsilon}_{k-1,C})^{-(d-4)/4}} \exp\left(\frac{\lambda}{2}r_k\right), \quad (10)$$

$$Z_{k,C} \approx \boldsymbol{\epsilon}_{k-1,C}^{-(d-1)/4} \exp(-\sqrt{\lambda}\boldsymbol{\epsilon}_{k-1,C}) \exp\left(\frac{\lambda}{2}r_k\right), \quad (11)$$

where we have made a change of variables before marginalizing out $2\Delta_k + r_k$ and we have used the limiting form of $K_\nu(z)$ as $z \rightarrow \infty$ (Abramowitz and Stegun, 1965). Eltoft et al. (2006) have called equation (10) multivariate Laplace distribution. When $d = 1$, equation (11) is exact and is a univariate Laplace distribution. Nevertheless, equation (11) is particularly useful when d is large as a cheap numerically stable alternative to $K_\nu(z)$.

3.1 Sampling coalescing times

Sampling from a generalized inverse Gaussian distribution is traditionally done using the *ratio-of-uniforms* method of Dagpunar (1989). We observed empirically that a slice sampler within the interval $(r_k/2, \Delta_0 r_k/2)$ is considerably faster than the commonly used algorithm. Although we use $\Delta_0 = 10^2$ in all our experiments, we did try larger values without noticing significant changes in the results. The slice sampler used here is a standard implementation of the algorithm described by Neal (2003b). We acknowledge that adaptively selecting Δ_0 at each step could improve the efficiency of the sampler however we did not investigate it.

3.2 Covariance matrix

Until now we assumed the covariance matrix Φ as known, in most cases however the correlation structure of the observed data is hardly available. In practice we need to alternate between SMC sampling for the tree structure and drawing Φ from some suitable distribution. For cases when observations exhibit additional structure, such as temporal or spatial data, we may assume the latent variable \mathbf{z}_k is drawn from a Gaussian process with mean \mathbf{z}_c and covariance function $\Delta_k g(i, j, \theta)$, where entries of Φ are computed using $\phi_{ij} = g(i, j, \theta)$ for a set of hyperparameters θ . For example, we could use a squared exponential covariance function

$$g(i, j, \ell, \sigma^2) = \exp\left(-\frac{1}{2\ell}d_{ij}^2\right) + \sigma^2\delta_{ij}, \quad (12)$$

where $\theta = \{\ell, \sigma^2\}$, $\delta_{ij} = 1$ only if $i = j$ and d_{ij} is the time between samples i and j . The covariance function in equation (12) is a fairly general assumption for continuous signals. The smoothness of the process is controlled by the inverse length scale ℓ and the amount of idiosyncratic noise by σ^2 . The elements of θ are sampled by coordinate-wise slice sampling using the following function as proxy for the elements of θ ,

$$f(\theta|\pi, \mathbf{t}) = \sum_{k=1}^{n-1} Z_k(\mathbf{X}|\pi_k, \mathbf{t}_{1:k}, \cdot).$$

For the case when no smoothness is required but correlation structure is expected, conjugate inverse Wishart distributions for Φ can be considered. For i.i.d. data, a diagonal/spherical Φ with independent inverse gamma priors is a good choice, as already proposed by Teh et al. (2008).

3.3 Greedy implementation

As pointed out by Teh et al. (2008), in some situations, a single good sample from the model is enough. Such a sample can be built by greedily maximizing equation (4) one step at the time. This requires the computation of the mode of Δ_k from equation (8) for every pair in π_{k-1} to then merge the pair with smallest Δ_k , so

$$\begin{aligned} \Delta_{k,C} &= \frac{1}{2\lambda} \left(\tilde{\lambda} + \sqrt{\tilde{\lambda}^2 + \lambda\epsilon_{k-1,C}} \right) - \frac{1}{2}r_k, \\ C^* &= \underset{\rho}{\operatorname{argmin}} \{ \Delta_{k,C}, C \in \pi_{k-1} \}. \end{aligned}$$

The greedy algorithm proposed by Teh et al. (2008) uses instead

$$\Delta_{k,C}^{\text{prev}} = \frac{1}{2\lambda} \left(-d + \sqrt{d^2 + 2\lambda\epsilon_{k-1,C}} \right) - \frac{1}{2}r_k.$$

The former proposal uses equation (8) whereas the latter uses equation (5) directly without taking into account $Z_{k,C}$. This means that using the properly normalized

posterior of Δ_k leads only to a minor correction of $\Delta_{k,C}$. The following Lemma 1 formalizes the relationship between the two proposals.

Lemma 1. *If $0 < \epsilon_{k-1,C} < \infty$, then the following holds*

1. $\Delta_{k,C}/\Delta_{k,C}^{\text{prev}} \rightarrow 1$ as $d \rightarrow \infty$.
2. $\Delta_{k,C}/\Delta_{k,C}^{\text{prev}} > 1$ if $\lambda\epsilon_{k-1,C} > 4(d+2)$.
3. $\Delta_{k,C} - \Delta_{k,C}^{\text{prev}}$ decreases as $2\lambda\epsilon_{k-1,C}/d^2 + \mathcal{O}(d^{-3})$.

Proof. For (1) is enough to take $\lim_{d \rightarrow \infty} \Delta_{k,C}/\Delta_{k,C}^{\text{prev}}$ by repeatedly applying L'Hospital's rule. (2) is obtained as the solution to the following system of equations

$$\begin{aligned}\tilde{\Delta}_{k,C}^2 + 2d\tilde{\Delta}_{k,C} &= 2\lambda\epsilon_{k-1,C}, \\ \tilde{\Delta}_{k,C}^2 + (d-2)\tilde{\Delta}_{k,C} &= \lambda\epsilon_{k-1,C},\end{aligned}$$

with solution $\Delta_{k,C} = 2 - r_k/2$ and $\lambda\epsilon_{k-1,C} = 4(d+2)$ for $\tilde{\Delta}_{k,C} = (2\Delta_{k,C} + r_k)$. Lastly, (3) is the result of a Taylor series expansion of $\Delta_{k,C} - \Delta_{k,C}^{\text{prev}}$. \square

Lemma 1 implies that $\Delta_{k,C}^{\text{prev}}$ only matches the true maximum a-posteriori estimate, $\Delta_{k,C}$, when $\lambda\epsilon_{k-1,C} = 4(d+2)$, thus $\Delta_{k,C}^{\text{prev}}$ is a biased estimator of \mathbf{t} almost everywhere. Besides, for small values of d , the difference between $\Delta_{k,C}$ and $\Delta_{k,C}^{\text{prev}}$ could be large enough to make the outcome of both algorithms significantly different.

3.4 Computational cost

The computational cost of using directly equation (5) to sample from \mathbf{t} and $\boldsymbol{\pi}$ for a single particle is $\mathcal{O}(\kappa_1 n^3)$, where κ_1 is the cost of drawing the merging time of a single candidate pair, as already mentioned by Teh et al. (2008). Using equation (6) costs $\mathcal{O}(\kappa_2 n^3 + \kappa_1 n)$, where κ_2 is the cost of computing $Z_{k,C}$ for a single candidate pair. Since $\kappa_2 \gg \kappa_1$, using equation (6) is much faster than what proposed by Teh et al. (2008), at least for moderately large n . From a closer look at equation (7) we see that the only variables changing with k are λ and r_k , but also that the only costly operation in it is the modified Bessel function provided we have previously cached $\epsilon_{.,C}$. We can approximate equation (7) by

$$Z_{k,C} \propto \frac{K_{\tilde{\lambda}}(\sqrt{\epsilon_{k-1,C}})}{(\epsilon_{k-1,C}^{-1})^{\tilde{\lambda}/2}} \exp\left(\frac{\lambda}{2} r_k\right), \quad (13)$$

this is, we have just dropped λ from the Bessel function and the divisor in equation (7), which is acceptable because (i) $K_\nu(z)$ is strictly decreasing for fixed ν and (ii) the λ term appearing in the divisor is a constant in $\log Z_{k,C}$. Note that a similar reasoning can be applied to equation (11), which is cheaper and more numerically stable. Since equation (13) does depend on k only through λr_k , we have virtually decreased the cost

from $\mathcal{O}(\kappa_2 n^3 + \kappa_3 n)$ to $\mathcal{O}(\kappa_2 n^2 + \kappa_3 n)$, that is, we need to compute equation (13) for every possible pair only once before selecting the merging pair at stage k , then we add $\lambda r_k/2$ (in log-domain) before sampling its merging time. From now on we use MPOST1 to refer to the algorithm using equation (6) and MPOST2 to the fast approximation in equation (13).

Recently, [Görür and Teh \(2009\)](#) proposed an efficient SMC sampler (SMC1) for hierarchical clustering with coalescents that although was introduced for discrete data can be easily adapted to continuous data. Their approach is based in a regenerative race process in which every possible pair candidate proposes a merging time only once leading to $\mathcal{O}(\kappa_1 n^2)$ computational time. In principle, SMC1 has quadratic cost as MPOST2, however since $\kappa_2 \gg \kappa_1$ our approximation is considerably faster. In addition, we have observed empirically that at least for n in the lower hundreds, MPOST1 is faster than SMC1 as well.

The key difference between our approach and that of [Görür and Teh \(2009\)](#) is that the latter proposes merging times for every possible pair and selects the pair to merge as the minimum available at a given stage whereas our approach selects the pair to merge and samples the merging time independently. Additionally, they do not sample merging times using $\Delta_k = t_k - t_{k-1}$ but directly $t_k|t_C$, where t_C is the time at which the pair C was created, thus $0 \leq t_C < t_k$. As t_C is usually smaller than t_{k-1} , SMC1 draw the vector \mathbf{t} in larger jumps compared to MPOST1/2. This suggests that our approach will have in general better mixing properties as we will show empirically in the next section.

4 Numerical results

In this section we consider a number of experiments on both artificial and real data to highlight the benefits of the proposed approaches as well as to compare them with previously proposed ones. In total three artificial data based simulations and two real data set applications are presented. All experiments are obtained using a desktop machine with 2.8GHz processor with 8GB RAM and run times are measured as single core CPU times.

4.1 Artificial data - structure

First we compare different sampling algorithms on artificially generated data using n -coalescents and Gaussian processes with known squared exponential covariance functions as priors. We generated 50 replicates of two different settings, D_1 and D_2 of sizes $\{n, d\} = \{32, 32\}$ and $\{64, 64\}$, respectively. We compare four different algorithms, POST-POST ([Teh et al., 2008](#)), SCM1 ([Görür and Teh, 2009](#)), MPOST1 and MPOST2. In each case we collect $M = 100$ particles and set the covariance function parameters $\{\ell, \sigma^2\}$ to their true values. As performance measures we track runtime (RT) as proxy to the computational cost, mean squared error (MSE), mean absolute error (MAE) and maximum absolute bias (MAB) of \mathbf{t} and $\boldsymbol{\pi}$ in log domain, as \mathbf{t} grows

Set	Measure	POST-POST	MPOST1	SMC1	MPOST2
Merge time (\mathbf{t})					
	$10^1 \times \text{MSE}$	0.52 ± 0.22	0.44 ± 0.18	0.66 ± 0.28	0.45 ± 0.18
D_1	$10^1 \times \text{MAE}$	1.88 ± 0.45	1.68 ± 0.39	2.01 ± 0.46	1.72 ± 0.40
	$10^1 \times \text{MAB}$	5.13 ± 1.23	4.93 ± 1.12	6.09 ± 1.30	4.91 ± 1.08
	$10^2 \times \text{MSE}$	4.06 ± 1.08	3.04 ± 0.90	5.37 ± 2.23	3.30 ± 0.94
D_2	$10^1 \times \text{MAE}$	1.73 ± 0.26	1.42 ± 0.26	1.83 ± 0.39	1.49 ± 0.27
	$10^1 \times \text{MAB}$	4.47 ± 0.73	4.40 ± 0.78	5.97 ± 1.39	4.39 ± 0.73
Distance matrix ($\boldsymbol{\pi}$)					
	$10^1 \times \text{MSE}$	0.79 ± 0.50	0.70 ± 0.49	1.32 ± 0.63	0.70 ± 0.42
D_1	$10^1 \times \text{MAE}$	2.24 ± 0.78	2.13 ± 0.76	3.03 ± 0.90	2.14 ± 0.72
	$10^1 \times \text{MAB}$	6.77 ± 1.20	6.50 ± 1.12	8.77 ± 1.96	6.48 ± 1.13
	$10^2 \times \text{MSE}$	5.79 ± 3.15	4.89 ± 2.92	11.36 ± 5.68	5.27 ± 2.94
D_2	$10^1 \times \text{MAE}$	1.95 ± 0.68	1.78 ± 0.65	2.85 ± 0.83	1.85 ± 0.65
	$10^1 \times \text{MAB}$	6.06 ± 0.79	5.75 ± 0.73	8.54 ± 2.01	5.81 ± 0.69
Computational cost					
D_1	$10^0 \times \text{RT}$	18.65 ± 0.24	2.29 ± 0.04	3.76 ± 0.07	1.98 ± 0.03
D_2	$10^{-1} \times \text{RT}$	14.50 ± 0.06	1.08 ± 0.00	1.39 ± 0.01	0.61 ± 0.00

Table 1: Performance measures for structure estimation. MSE, MAE, MAB and RT are mean squared error, mean absolute error and maximum absolute bias, and runtime in seconds, respectively. Figures are means and standard deviations across 50 replicates. Best results are in boldface letters.

exponentially fast. For the latter we compute the distance matrix encoded by $\{\mathbf{t}, \boldsymbol{\pi}\}$. Table 1 shows performance measures averaged over 50 replicates for each data set. In terms of error, we see that all four algorithms perform about the same, however with MPOST1 and SMC1 being slightly better and slightly worse, respectively. The computational cost is significantly higher for the POST-POST approach whereas MPOST2 is the fastest. We see MPOST1 and MPOST2 consistently outperforming the other two algorithms as an indication of better mixing properties. In more general terms, MPOST2 provides the best error/computational cost trade-off as the difference in accuracy between MPOST1 and MPOST2 is rather minimal.

4.2 Artificial data - covariance

Next we want to test the different sampling algorithms when the parameters of the Gaussian process covariance function, $\{\ell, \sigma^2\}$, need to be learned as well. We use settings similar to those in the previous experiment with the difference that now $M = 50$ particles are collected and $N_{\text{iter}} = 50$ iterations are performed to learn the covariance matrix parameters. We dropped the first 10 iterations as burn-in period. In addition to the previously mentioned performance measures we also compute MSE, MAE and MAB for the inverse length scale ℓ from equation (12). In order to simplify the experiment

Set	Measure	MPOST1	SMC1	MPOST2
Merge time (t)				
	$10^1 \times \text{MSE}$	1.20 ± 0.51	1.26 ± 0.44	1.24 ± 0.53
D_1	$10^1 \times \text{MAE}$	3.02 ± 0.80	2.98 ± 0.62	3.06 ± 0.81
	$10^1 \times \text{MAB}$	6.43 ± 1.26	7.01 ± 1.50	6.52 ± 1.38
	$10^2 \times \text{MSE}$	5.38 ± 1.66	6.32 ± 1.94	5.61 ± 1.76
D_2	$10^1 \times \text{MAE}$	2.02 ± 0.36	2.01 ± 0.36	2.07 ± 0.36
	$10^1 \times \text{MAB}$	4.75 ± 0.72	6.16 ± 1.35	4.73 ± 0.62
Distance matrix (π)				
	$10^1 \times \text{MSE}$	1.31 ± 0.87	2.85 ± 1.76	1.33 ± 0.86
D_1	$10^1 \times \text{MAE}$	2.94 ± 1.19	4.53 ± 1.69	2.96 ± 1.19
	$10^1 \times \text{MAB}$	8.77 ± 2.18	9.60 ± 1.73	8.84 ± 2.13
	$10^1 \times \text{MSE}$	0.64 ± 0.35	1.54 ± 0.67	0.66 ± 0.34
D_2	$10^1 \times \text{MAE}$	2.08 ± 0.63	3.29 ± 0.94	2.08 ± 0.65
	$10^1 \times \text{MAB}$	6.77 ± 1.13	8.41 ± 1.42	6.76 ± 1.15
Inverse length scale (ℓ)				
	$10^4 \times \text{MSE}$	2.36 ± 3.20	2.93 ± 4.51	2.38 ± 3.23
D_1	$10^2 \times \text{MAE}$	1.17 ± 0.99	1.24 ± 1.09	1.18 ± 0.99
	$10^2 \times \text{MAB}$	1.40 ± 1.14	2.06 ± 2.18	1.38 ± 1.15
	$10^4 \times \text{MSE}$	2.86 ± 3.22	3.55 ± 4.48	2.83 ± 3.17
D_2	$10^2 \times \text{MAE}$	1.35 ± 1.02	1.44 ± 1.14	1.34 ± 1.01
	$10^2 \times \text{MAB}$	1.57 ± 1.29	2.39 ± 2.24	1.55 ± 1.27
Computational cost				
D_1	$10^{-1} \times \text{RT}$	5.69 ± 0.02	13.65 ± 0.06	4.86 ± 0.02
D_2	$10^{-2} \times \text{RT}$	2.72 ± 0.07	5.12 ± 0.05	1.49 ± 0.01

Table 2: Performance measures for covariance estimation. MSE, MAE, MAB and RT are mean squared error, mean absolute error and maximum absolute bias, and runtime in seconds, respectively. Figures are means and standard deviations across 50 replicates. Best results are in boldface letters.

we set a priori $\sigma^2 = 1 \times 10^{-9}$ to match a *noiseless* scenario, however similar results are obtained when learning both parameters at the same time (results not shown). Table 2 shows an overall similar trend when compared to Table 1. In terms of covariance function parameter estimation, we see all algorithms perform about the same which is not surprising considering they use the same sampling strategy.

4.3 Artificial data - greedy algorithm

As final simulation based on artificial data we want to test whether the correction to the greedy algorithm of Teh et al. (2008) makes any differences performance-wise. We generated 50 replicates of two different settings D_1 and D_2 of sizes $\{n, d\} = \{32, 32\}$ and $\{128, 128\}$, respectively. We run N_{iter} iterations of the algorithm and drop the first 10

Measure	D_1		Measure	D_2	
	GREEDY	MGREEDY		GREEDY	MGREEDY
Merge time (t)					
$10^1 \times \text{MSE}$	1.26 ± 0.48	0.90 ± 0.36	$10^2 \times \text{MSE}$	0.98 ± 0.23	0.78 ± 0.19
$10^1 \times \text{MAE}$	3.10 ± 0.67	2.53 ± 0.59	$10^1 \times \text{MAE}$	0.81 ± 0.11	0.71 ± 0.10
$10^1 \times \text{MAB}$	7.03 ± 1.54	6.38 ± 1.50	$10^1 \times \text{MAB}$	2.74 ± 0.49	2.59 ± 0.49
Distance matrix (π)					
$10^1 \times \text{MSE}$	1.33 ± 0.74	1.02 ± 0.60	$10^1 \times \text{MSE}$	0.14 ± 0.11	0.12 ± 0.09
$10^1 \times \text{MAE}$	3.04 ± 1.02	2.58 ± 0.93	$10^1 \times \text{MAE}$	0.95 ± 0.38	0.87 ± 0.35
$10^1 \times \text{MAB}$	8.90 ± 1.70	8.24 ± 1.69	$10^1 \times \text{MAB}$	4.05 ± 0.69	3.90 ± 0.68
Inverse length scale (ℓ)					
$10^4 \times \text{MSE}$	2.03 ± 2.61	2.03 ± 2.58	$10^4 \times \text{MSE}$	2.79 ± 3.54	2.79 ± 3.56
$10^2 \times \text{MAE}$	1.10 ± 0.91	1.10 ± 0.90	$10^2 \times \text{MAE}$	1.32 ± 1.03	1.32 ± 1.03
$10^2 \times \text{MAB}$	1.24 ± 1.00	1.24 ± 0.99	$10^2 \times \text{MAB}$	1.39 ± 1.06	1.43 ± 1.15
Computational cost					
$10^0 \times \text{RT}$	1.65 ± 0.09	1.66 ± 0.08	$10^{-1} \times \text{RT}$	3.86 ± 2.42	3.79 ± 2.31

Table 3: Performance measures for greedy algorithms. MSE, MAE, MAB and RT are mean squared error, mean absolute error and maximum absolute bias, and runtime in seconds, respectively. Figures are means and standard deviations across 50 replicates. Best results are in boldface letters.

samples as burn-in period. The performance measures are the same as in the previous experiment. Table 3 shows that the corrected algorithm performs consistently better than the original when the data set is small. When the data set is larger the difference between the two algorithms diminishes however still favors MGREEDY. Although not shown, we tried other settings in between D_1 , D_2 and larger than D_2 with consistent results, this is, the difference between GREEDY and MGREEDY decreases with the size of the dataset.

4.4 Handwritten digits

The USPS database¹ contains 9289 grayscale images of 16×16 pixels in size, scaled to fall within the range $[-1, 1]$. Here we use subsets of 500 images, 50 from each digit, randomly selected from the full data set. We apply MPOST2, MGREEDY and average-link agglomerative clustering (HC) to 25 of such subsets. For the covariance matrix Φ we use a Matérn covariance function with parameter $\nu = 3/2$ and additive noise defined as follows

$$g(i, j, \ell_x, \ell_y, \sigma^2) = \left(1 + \frac{\sqrt{3}}{\ell_x} d_{x,ij}\right) \left(1 + \frac{\sqrt{3}}{\ell_y} d_{y,ij}\right) \exp\left(-\frac{\sqrt{3}}{\ell_x} d_{x,ij} + \frac{\sqrt{3}}{\ell_y} d_{y,ij}\right) + \sigma^2 \delta_{ij},$$

¹Data available from <http://cs.nyu.edu/~roweis/data.html>.

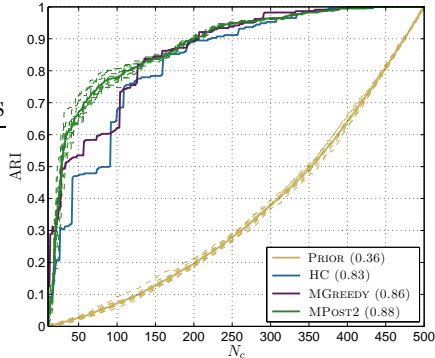


Figure 2: USPS digits results. (Left) USPS data ARI curves. PRIORITY draws structures directly from a n -coalescent prior and HC is standard hierarchical clustering with average link function and euclidean distance metric. Figures in parenthesis are AUC scores. (Right) Subtree scores, AUC is area under the ARI curve and RT is runtime in minutes. Figures are means and standard deviations across 25 replicates. Best results are in boldface letters.

where $d_{x,ij}$ and $d_{y,ij}$ are distances in the two axes of the image, and we have assumed axis-wise independency (Rasmussen and Williams, 2006).

4.4.1 Performance metrics

As performance measures we use (i) the *subtree* score defined as $N_{\text{subset}}/(n - C)$, where N_{subset} is the number of internal nodes with leaves from the same class and C is the number of classes (Teh et al., 2008), and (ii) the area under the adjusted Rand index (ARI) curve (AUC). ARI is a similarity measure for pairs of data partitions that take values between 0 and 1, the latter indicating that the two partitions are exactly the same (Hubert and Arabie, 1985). Although ARI has been extensively used for clustering assessment, its use in hierarchical clustering requires the tree to be cut to obtain a single partition of data. Provided we can obtain n different partitions from hierarchical clustering on n observations, we can compute ARI for all partitions using a majority voting rule to label internal nodes of the tree structure. If we plot ARI vs number of clusters N_c we obtain a graphical representation that resembles a ROC curve. When all partitions have a correct label, ARI will be 1 for $N_c > C$ and in any other case, ARI will increase with N_c . Besides, when $N_c = 1$ and $N_c = n$, ARI is always 0 and 1, respectively. Just like in a ROC curve, an algorithm is as good as its ARI's rate of change thus we can assess the overall performance by computing the area under the ARI curve. Figure 2 shows curves for a particular data set and the three considered algorithms. We also included results obtained by tree structures drawn from the coalescent prior as reference.

Table in Figure 2 shows average subset scores for the algorithms considered. We performed inference for 20 iterations and 10 particles. Not substantial improvement was found by increasing N_{iter} or M . GREEDY produced the same results as MGREEDY

and SMC1 did not performed better than MPOOST1/2 but it took approximately 10 times longer to run (results not shown). We see that coalescent based algorithms perform considerable better than standard hierarchical cluster in terms of AUC. Besides, MPOST1 and MPOST2 are best in subtree scores and AUC, respectively.

4.5 Motion capture data

We apply MPOST2 to learn hierarchical structures in motion capture data (MOCAP). The data set consist of 102 time series of length 217 corresponding to the coordinates of a set of 34 three dimensional markers placed on a person breaking into run². For the covariance matrix Φ , we used the squared exponential function in equation (12). Results are obtained after running 50 iterations of MPOST2 with 50 particles. It took approximately 5 minutes to complete the run. Left panel in Figure 3 shows two subtrees containing data from all markers in the X and Z axes. Aiming to facilitate visualization, we relabeled the original markers to one of the following: head (Head), torso (Torso), right leg (Leg:R), left leg (Leg:L), right arm (Arm:R) and left arm (Arm:L). The subtrees from Figure 3 are obtained from the particle with maximum weight (0.129) at the final iteration of the run with effective sample size 24.108. We also examined the trees for the remaining particles and noted no substantial structural differences with respect to Figure 3. The resulting tree has interesting features: (i) Sensors from different coordinates are put together. (ii) Leg markers have in general larger merging times than the others, whereas the opposite is true for head markers. (iii) The obtained tree fairly agrees with the structure of the human body, for instance in the middle-right panel of Figure 3 we see a heat map with 9 markers, 4 of them from the head, 1 from the torso (C7, base of the neck) and 4 from the arms (shoulders and upper arms). The two arm sensors close to the torso correspond to the shoulders while the other two—with larger merging times, are located in the upper arms. We observed that the obtained structure is fairly robust to changes in the number of iterations and particles. We also point out that MPOST1, GREEDYNEW, SMC1, and POST produce structurally similar trees to the one shown in Figure 3, however with different running times. In particular, they took 7, 1, 12 and 75 minutes, respectively.

5 Discussion

The model for hierarchical clustering for continuous data presented in this paper has shown to perform better than the other alternatives available in the literature with appealing reduced computational cost. We also showed that the approximation MPOST2 has nearly the same performance as the exact version MPOST1 but with much improved computational cost and that the greedy strategy obtained as the mode of the merging time posterior behaves better than the algorithm proposed by Teh et al. (2008). Experiments with real data highlight the flexibility of our model by means of exploiting

²Data available from http://accad.osu.edu/research/mocap/mocap_data.htm.

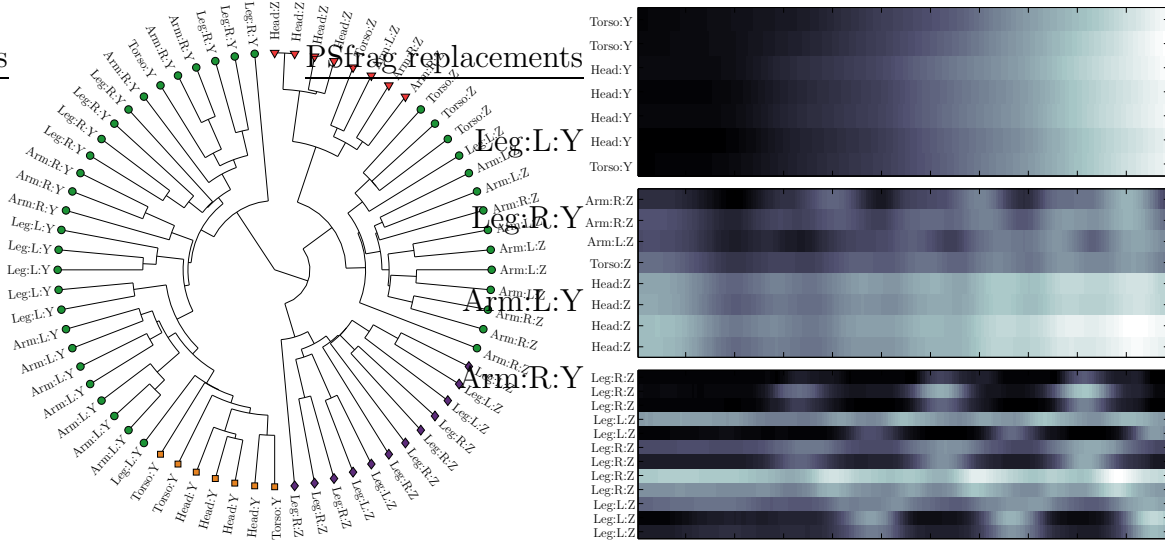


Figure 3: MOCAP data results. (Left) Resulting subtree from the particle with maximum weight (0.0784) at iteration 50. (Right) Data corresponding to three subtrees of (Left) marked with squares, triangles and diamonds, respectively.

covariation through the use of Gaussian process priors.

Some opportunities for future research being considered include: use the hierarchical cluster model as a prior for the factors in a factor model for better handling of time series or replicates in biological data. The model itself could see improvements if allowed for arbitrary branching structures and stage specific length scales.

Supplementary materials

Source code: Matlab/C code required to perform the methods described in the manuscript, including sample scripts and the artificial data generator used throughout the results section ([mvbtree_v0.1.zip](#), compressed file).

A Tree posteriors details

We can write the first line of equation (6) as

$$= p(\Delta_k | \pi_k, \mathbf{t}_{1:k-1}, \cdot) p(\pi_k | \mathbf{t}_{1:k-1}, \pi_{k-1}, \cdot), \quad (14)$$

$$= \mathcal{N}(\mathbf{m} | \mathbf{0}, v_k \Phi) \text{Exponential}(v_k | \lambda/2) \text{Exponential}(-r_k | \lambda/2),$$

$$= \frac{\lambda}{2} (2\pi)^{-d/2} |\Phi|^{-1/2} |v_k|^{-1/2} \underbrace{\exp\left(-\frac{1}{2} v_k^{-1} \boldsymbol{\epsilon}_{k-1,C} - \frac{1}{2} \lambda v_k\right)}_{\text{core of a generalized inverse Gaussian}} \frac{\lambda}{2} \exp\left(\frac{\lambda}{2} r_k\right), \quad (15)$$

where $\lambda = (n - k + 1)(n - k)/2$, $\mathbf{m} = \mathbf{m}_{c_1} - \mathbf{m}_{c_2}$ and $\boldsymbol{\epsilon}_{k-1,C} = \mathbf{m} \Phi^{-1} \mathbf{m}^\top$. We recognize the segment in braces of equation (15) as the core of a generalized inverse Gaussian

distribution (Jørgensen, 1982) defined as

$$\text{GIG}(x|\lambda, \chi, \psi) = \frac{(\psi\chi^{-1})^{\lambda/2}}{2K_\lambda(\sqrt{\psi\chi})} x^{\lambda-1} \exp\left(-\frac{\chi}{2}x^{-1} - \frac{\psi}{2}x\right),$$

where $K_\nu(z)$ is the modified Bessel function of second kind with parameter ν .

We can thus rewrite equation (14) as

$$\begin{aligned} \Delta_k|\pi_k, \mathbf{t}_{1:k-1}, \cdot &\sim \text{GIG}(v_k|\tilde{\lambda}, \epsilon_{k,C}, \lambda), \\ \pi_k|\mathbf{t}_{1:k-1}, \pi_{k-1}, \cdot &\propto \underbrace{\frac{\lambda^2}{4}(2\pi)^{-d/2} \frac{2K_{\tilde{\lambda}}(\sqrt{\lambda\epsilon_{k-1,C}})}{(\lambda\epsilon_{k-1,C}^{-1})^{\tilde{\lambda}/2}} |\Phi|^{-1/2} \exp(\frac{\lambda}{2}r_k)}_{Z_{k,C}}, \end{aligned}$$

where $\tilde{\lambda} = 1 - d/2$.

References

- M. Abramowitz and I. A. Stegun. *Handbook of mathematical functions: with formulas, graphs, and mathematical tables*. Dover Publications, New York, 1965.
- R. P. Adams, Z. Ghahramani, and M. I. Jordan. Tree-structured stick breaking for hierarchical data. In J. Lafferty, C. K. I. Williams, J. Shawe-Taylor, R. S. Zemel, and A. Culotta, editors, *Advances in Neural Information Processing Systems 23*, pages 19–27. MIT Press, 2010.
- J. S. Dagpunar. An easily implemented generalised inverse Gaussian generator. *Communications in Statistics - Simulation and Computation*, 18(2):703–710, 1989.
- A. Doucet, N. de Freitas, N. Gordon, and A. Smith. *Sequential Monte Carlo Methods in Practice*. Springer, 2001.
- T. Eltoft, T. Kim, and T.-W. Lee. On the multivariate Laplace distribution. *IEEE Signal Processing Letters*, 13(5):300–303, 2006.
- D. Görür and Y. W. Teh. An efficient sequential Monte Carlo algorithm for coalescent clustering. In D. Koller, D. Schuurmans, Y. Bengio, and L. Bottou, editors, *Advances in Neural Information Processing Systems 21*, pages 521–528. MIT Press, 2009.
- K. A. Heller and Z. Ghahramani. Bayesian hierarchical clustering. In *Proceedings of the 22nd international conference on Machine learning*, pages 297–304. ACM, 2005.
- R. Henao, J. W. Thompson, M. A. Moseley, G. S. Ginsburg, L. Carin, and J. E. Lucas. Hierarchical factor models for proteomics data. In *Computational Advances in Bio and Medical Sciences (ICCBAS), 2012 IEEE 2nd International Conference on*, 2012.

- L. Hubert and P. Arabie. Comparing partitions. *Journal of Classification*, 2(1):193–218, 1985.
- Bent Jørgensen. *Statistical properties of the generalized inverse Gaussian distribution*, volume 9 of *Lecture notes in statistics*. Springer-Verlag, 1982.
- J. F. C. Kingman. The coalescent. *Stochastic processes and their applications*, 13(3):235–248, 1982a.
- J. F. C. Kingman. On the genealogy of large populations. *Journal of Applied Probability*, 19:27–43, 1982b.
- R. Neal. Density modeling and clustering using Dirichlet diffusion trees. In J. Bernardo, M. Bayarri, J. Berger, A. Dawid, D. Heckerman, A. Smith, and M. West, editors, *Bayesian Statistics 7*, pages 619–629. Oxford University Press, 2003a.
- R. M. Neal. Slice sampling. *Annals of Statistics*, 31(3):705–741, 2003b.
- J. Pearl. *Probabilistic Reasoning in Intelligent Systems: Networks of Plausible Inference*. Morgan Kaufmann, 1988.
- P. Rai and H. Daume III. The infinite hierarchical factor regression model. In D. Koller, D. Schuurmans, Y. Bengio, and L. Bottou, editors, *Advances in Neural Information Processing Systems 21*, pages 1321–1328. MIT Press, 2009.
- C. E. Rasmussen and C. K. I. Williams. *Gaussian Processes for Machine Learning*. The MIT Press, Cambridge, MA, 2006.
- Y. W. Teh, H. Daume III, and D. Roy. Bayesian agglomerative clustering with coalescents. In J. C. Platt, D. Koller, Y. Singer, and S. T. Roweis, editors, *Advances in Neural Information Processing Systems 20*, pages 1473–1480. MIT Press, 2008.
- X. Zhang, D. Dunson, and L. Carin. Tree-structured infinite sparse factor model. In L. Getoor and T. Scheffer, editors, *Proceedings of the 28th International Conference on Machine Learning (ICML-11)*, pages 785–792, 2011.